A new Approach for Positioning Integrity Monitoring of Intelligent Transport Systems Using Integrated RTK-GNSS, IMU and Vehicle Odometer

Ahmed El-Mowafy[1*], Nobuaki Kubo[2]

[1] School of Earth and Planetary Sciences, Curtin University, GPO Box U 1987, Perth WA 6845, Australia
[2] Department of Maritime Systems Engineering, Tokyo University of Marine Science and Technology, Tokyo, Japan.

* a.El-Mowafy@curtin.edu.au,

Abstract: Reliable continuing positioning is a critical requirement for Intelligent Transportation Systems (ITS). An integrated positioning system is presented in this study, where the Global Navigation Satellite Systems (GNSS) Real-Time Kinematic (RTK) method was mainly used. When RTK is not available, positioning was maintained by a method using Doppler measurements or by using low-cost inertial measurement unit (IMU) coupled with car odometer measurements. A new integrity monitoring method is presented that addresses each positioning mode of the proposed integrated system. Models for the protection levels are presented to bound the position error along the direction of motion of the vehicle and for the cross-track direction. Both direction components are needed for ITS, for instance, for collision avoidance and for lane identification. The method was assessed through a kinematic test performed in a dense urban environment. Results showed that by integrating GNSS RTK, Doppler with IMU+odometer, positioning was available all the time. For RTK, positioning accuracy was less than a decimetre and the integrity monitoring availability met our target threshold of 99%, where the protection levels bounded the position errors and were less than an alert limit of 1 m. Positioning using Doppler and IMU+odometer measurements bridged RTK breaks but at the sub-meter level accuracy when used for short periods.

1. Introduction

Intelligent Transport systems (ITS) require continuous precise vehicle positioning in real time. They mainly relay on GNSS for positioning. However, buildings and other obstacles can obstruct signals, in particular in urban environment [1], thus GNSS needs to be integrated with other sensors such as inertial measurement units (IMUs) to bridge positioning during GNSS positioning breaks [2, 3]. In ITS, positioning is needed to the sub-metre accuracy level for in-lane positioning. Such accuracy can be achieved with methods such as Real-Time Kinematic (RTK) [4], Precise Point Positioning (PPP) [5, 6], and Satellite Based Augmentation Systems (SBAS). In this article we consider the use of GNSS integrated with low-cost IMU and measurements from vehicle odometer. RTK is currently under consideration by car manufacturers driven by the rapid decline of receiver cost and the development of economy single-frequency, and even dual-frequency, systems that can achieve a few cm to sub-m accuracy. However, the inexpensive Micro-electro-mechanical systems (MEMS) IMUs that can be used in vehicle applications yield a heading bias that quickly grows with time. Such a bias can be adjusted by heading data computed from GNSS Doppler observations when they are available. These methods can only estimate position changes with time, and hence, their positioning errors accumulate with time. Thus, they can only be used for positioning of short outages of RTK positioning.

For ITS safety-related applications, integrity monitoring (IM) is a key positioning performance parameter, where the system should be able to detect and exclude measurement faults, bound measurement errors, and trigger an alarm in the event that unreliable positioning performance is suspected. In addition, when no fault is detected, IM provides a protection level (PL) that should bound the true position error at a certain probability of risk [7]. Even though integrity requirements in vehicular transport have not been defined yet, the demand for higher levels of automation in an increasing number of applications is pushing the relevant authorities to urgently fill this gap.

IM is currently being applied in aviation using Advanced Receiver Autonomous Integrity Monitoring (ARAIM) approach, which relies on the use of multi-frequency and multi-constellation phase-smoothed pseudorange observations [8-10]. However, limited research has been done for applications that utilise carrier-phase observations used in RTK, taken into consideration the carrier-phase ambiguity resolution. Some examples are given in [11, 12] for relative positioning, in [13] for PPP, and in [14] for RTK.

So far, most IM proposed methods focused on applying ARAIM and only employing GNSS measurements. However, for ITS, GNSS cannot be used solely, and hence new IM methods are needed when integrating GNSS with other sensors [15]. In our earlier work [14], we discussed one method for positioning IM when RTK was integrated with low-cost IMU, vehicle odometer and Doppler observations for advanced driver assistance systems (ADAS). The PLs that bound the position error were presented for an overall horizontal vector and for the maximum-direction positioning component. In this contribution, a new model is presented for computation of the PLs, restricting our focus to horizontal positioning for the along-track and cross-track positioning components of the vehicles, which are of interest for forward collision warning, which is a major risk condition, and for in-lane identification. The PL models are developed for continuous positioning for vehicular applications is proposed

El-Mowafy, A., Kubo, N. (2018) Integrity monitoring for Positioning of intelligent transport systems using integrated RTK-GNSS, IMU and vehicle odometer, IET Intelligent Transport Systems 12(8): 901 –908

by integrating RTK GNSS using code and phase observations supplemented by simple approaches using Doppler measurements, low-cost IMU, and vehicle odometer data.
.
The structure of the paper is organised as follows. The next section briefly overviews the positioning methods considered in this research. In Section 3, the proposed integrity monitoring method for the three positioning modes under consideration is presented. In section 4, the proposed method is evaluated using a kinematic test in a dense urban environment. Finally, the conclusion and future work are given.

2. Positioning Modes

The fault-free observation equation can be expressed as:

$$y = G\,x + b + \varepsilon \quad (1)$$

where y is the measurement vector, computed as the difference between the observations and their estimated values from the approximate position of the user. The null hypothesis is expressed as H_0: $E\{y\} = G\,x + b$ with $D\{y\} = Q_y$, representing the covariance matrix of the observations, where $E\{\}$ and $D\{\}$ symbolize the expectation and dispersion operators. The unknown vector x is the difference between the final and approximate vehicle's computed positions. b is the nominal biases (not considering outliers) and ε is the observation noise [14].

An RTK mode with a single reference station is considered in this study, where the vehicle receiver operates within a few kilometres from the reference receiver such that the broadcast orbital error and the atmospheric delays (ionosphere and troposphere) are cancelled by double-differencing the observations, leading to ±5 cm accuracy [16]. Similarly, a network RTK approach [17] can be applied. To achieve such accuracy, five or more satellites with a good geometry should be tracked when using one GNSS system and more than two satellites for each additional system to resolve the ambiguities on-the-fly. The G matrix is the geometry-design matrix, computed from the approximate position of the user and broadcast satellite positions.

When the number of tracked satellites is reduced to our for a single GNSS system, for instance due to signal obstruction, and to bridge short RTK positioning gaps, the velocity computed from GNSS Doppler measurements can be time integrated to estimate changes in vehicle locations with time where the initial position can be determined from RTK. Consequently, the unknowns become the time change of E and N, denoted by ΔE and ΔN and the vehicle position at time t is then expressed as:

$$E_t = E_{t-1} + \Delta E \quad \text{and} \quad N_t = N_{t-1} + \Delta N. \quad (2)$$

where the G matrix reads:

$$G = \frac{1}{\Delta t} \times \mathrm{I} \quad (3)$$

I is the identity matrix. Positioning in this case is dependent on geometry of the tracked satellites and accuracy of the computed speed of the vehicle. This accuracy is a function of the vehicle speed itself. When the vehicle is stationary, the observed Doppler measurements would represent noise. The second column in Table 1 summarises the empirical conditions, set based on our experimental testing, to avoid undesirable false jumps in the estimated velocity and to bound positioning errors to under 1 m for short breaks in RTK positioning. The shown V_{GNSS} represents the speed estimated from GNSS Doppler observations.

Table 1. Empirical conditions for using different positioning modes

RTK	Using Doppler observations	Doppler calibrating IMU+odometer
• HDOP < 3	• $\lvert V_{GNSS} - V_{SS}\rvert$ < 0.5 m/s • (HDOP) < 1.5	• The odometer speed > 0.5 m/s; • $\lvert V_{GNSS} - V_{SS}\rvert$ < 1.5 m/s; • HDOP < 2.5

If RTK or positioning using Doppler observations are unavailable, the positions can be estimated by integrating the speed estimated from the vehicle odometer (expressed as the scalar V_{SS}) with the heading of the MEMS IMU, denoted as θ. The Easting and Northing velocity components are computed as $V_E = \sin(\theta) \times V_{ss}$, and $V_N = \cos(\theta) \times V_{ss}$. These velocities are integrated in time to provide the position time changes in Easting and Northing directions, where the position is computed using (2). The observations are considered in this case as the mean values of the IMU heading (θ) and the odometer speed, for instance between the epochs *t-1* and *t*. Thus, the G matrix is expressed as:

$$G_t = \begin{bmatrix} \frac{\partial\,\theta}{\partial \Delta E} & \frac{\partial\,\theta}{\partial \Delta N} \\ \frac{\partial\,v}{\partial \Delta E} & \frac{\partial\,v}{\partial \Delta N} \end{bmatrix}_t = \begin{bmatrix} \frac{\Delta N}{\Delta E^2 + \Delta N^2} & \frac{-\Delta E}{\Delta E^2 + \Delta N^2} \\ \frac{\Delta E}{\Delta t \times \sqrt{\Delta E^2 + \Delta N^2}} & \frac{\Delta N}{\Delta t \times \sqrt{\Delta E^2 + \Delta N^2}} \end{bmatrix}_t \quad (4)$$

As mentioned earlier, the IMU heading bias is cumulative; accordingly, it should be frequently calibrated. When Doppler velocities are available, they can be used to compute the initial values of IMU heading and for calibration of the IMU heading, that can applied at short intervals to control the growth of this bias [18-20]. The computed heading from Doppler measurements at time t (denoted as θ_t) is calculated from $\theta_t = tan^{-1}\left(\frac{V_{E_t}}{V_{N_t}}\right)$, where V_{E_t} and V_{N_t} denote the velocity components in the local-level frame. The operational empirical conditions for this case to keep the heading error to below 2 degrees are listed in the third column in Table 1. If these conditions are not met, or when Doppler measurements are not available, the IMU is calibrated when the vehicle is stationary by applying a Zero-velocity update (ZUPT).
Figure 1 shows a flowchart of the positioning approach proposed in this simple system [14], where it is applied in the

following order depending on fulfilment of the set empirical conditions given in Table 1: RTK; henceforth using Doppler measurements; and last using MEMS IMU coupled with odometer data. The latter two methods have positioning error that increases with time; thus, they should only be restricted to bridging short breaks in RTK.

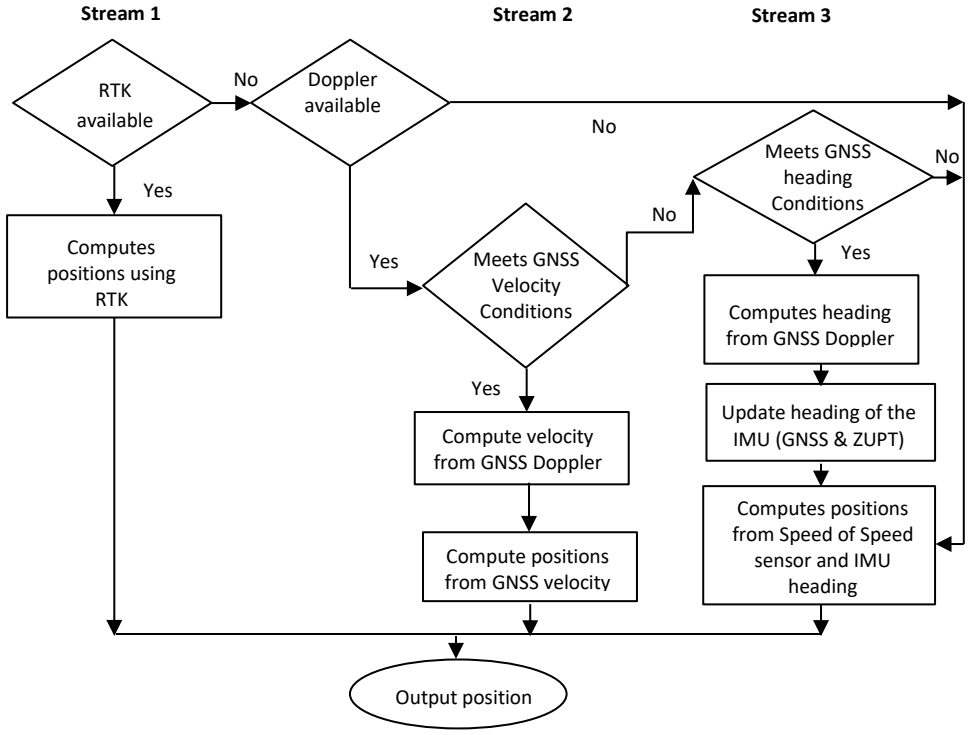

Fig. 1. Flowchart of positioning using the integrated RTK GNSS/IMU/odometer system [14]

3. Integrity Monitoring

In IM, the system is monitored to detect and exclude faults in the observations. Next, the protection levels (PLs) that bound the true position errors with a probability that does not exceed the allowable integrity risk are computed. When each PL does not exceed a threshold (alert limit), IM is considered available. In this section, a summary of the integrity monitoring for the presented system is given.

3.1. Detection and exclusion of faulty observations

In the presence of suspected faults, or large errors, denoted here as ∇, the observation model can be expressed as:

$$y = G\,x + C\,\nabla + b + \varepsilon \tag{5}$$

which gives the alternative hypothesis H_a: $\mathrm{E}\{y\} = G\,x + C\,\nabla + b$. In principle, detection of these faults can be performed by applying a consistency check among all possible sets of observations. Hence, we can only detect faults when positioning can be available from at least one set of error-free observations. Accordingly, we can detect up to q number of faults when $1 \leq q \leq df$, where *df* is the degrees of freedom. In (5), C is a matrix that describes which observations are suspected to be faulty. For *m* observations, C will have $m \times q$ dimension, where each of its columns has a one corresponding to the observation assumed to be affected by a fault and zeros elsewhere. The matrix should be set to test all possibilities of the presence of errors in the observations. In RTK, due to the correlation between phase and code errors, cycle slips of phase observations are first detected and repaired and next code outliers are excluded [23]. Several methods are presented for cycle slip detection, for instance by using the time difference of the between phase observations from two frequencies or by monitoring the rate of change of the ionosphere delay [21, 22].

Utilizing the observation residuals, the best estimator of the error vector ($\hat{\nabla}$) can be determined from [24]:

$$\hat{\nabla} = (C^T Q_y^{-1} Q_{\hat{e}} Q_y^{-1} C)^{-1} C^T Q_y^{-1} \hat{e} \tag{6}$$

with its covariance matrix expressed as:

$$Q_{\hat{\nabla}} = (C^T Q_y^{-1} Q_{\hat{e}} Q_y^{-1} C)^{-1} \tag{7}$$

where $\hat{e}$ and $Q_{\hat{e}}$ are the computed observation residuals and their covariance matrix is computed as:
$Q_{\hat{e}} = Q_{\mathrm{y}} - [G(G^T Q_{\mathrm{y}}^{-1} G)^{-1} G^T]$.

The *uniformly most powerful invariant* (UMPI) test is applied for a quick detection of faults. Under the assumption that the observation errors (but not the outliers) are zero-mean Gaussian; the statistic ($\hat{\nabla}^T Q_{\hat{\nabla}}^{-1}\,\hat{\nabla}$) in the fault-free mode will have a Chi-square distribution. Accordingly, observation

errors are suspected when they exceed a certain threshold, i.e. when [24]:

$$\hat{V}^T Q_{\hat{V}}^{-1} \hat{V} \geq \chi^2_{\alpha 1}(df, 0) \quad (8)$$

where $\chi^2_{\alpha 1}(df, 0)$ is the Chi-square threshold computed at a given significance level – or a false alarm - ($\alpha 1$) and df. If the test fails, one needs to identify and exclude the suspected observations corresponding to the suspected faults.

Using least squares for fault detection, the solution of the unknown position expressed in the Easting-Northing-Up (E-N-U) frame reads:

$$\hat{x} = R\,(G^T\,Q_y^{-1}\,G)^{-1}\,G^T\,Q_y^{-1}\,y = S\;y \quad (9)$$

where $S = R\,(G^T\,Q_y^{-1}\,G)^{-1}\,G^T\,Q_y^{-1}$ is the pseudo inverse, which maps the observations onto the unknowns. In RTK, *R* is the rotation matrix from the Cartesian frame, in which the GNSS satellite positions are expressed, to the E-N-U frame. In the other two positioning scenarios, using Doppler observations and IMU + odometer measurements, *R* is the identity matrix. To identify which observations are faulty, the solution separation method can be applied [8]. For each potential fault mode *i*, which may include one or more observations. An analogous S_i matrix is computed by excluding the suspected observations as follows:

$$S_i = R\big(\,G^T\,(A_i\,Q_y^{-1})\,G\,)^{-1}\,G^T\,(A_i Q_y^{-1}\big) \quad (10)$$

where A_i is an identity matrix reformed such that the diagonal elements corresponding to the suspected faulty measurements in mode *i* are replaced by zero. The residual positional vector $|\hat{x} - \hat{x}_i|$ is then determined from (9) and:

$$\hat{x}_i = S_i\,y \quad (11)$$

The standard deviations of the difference between the two solutions $\hat{x}$ and $\hat{x}_i$ (denoted here as σ_{dE_i}, σ_{dN_i}, σ_{dU_i}) are next computed as:

$$\sigma_q = \sqrt{a_k^T\;(S_i - S)\,Q_y\,(S_i - S)^T\,a_k} \quad (12)$$

where *k=1, 2, 3* corresponding to dE_i, dN_i, dU_i such that $a_1^T = [1,0,0]$, $a_2^T = [0,1,0]$, and $a_3^T = [0,0,1]$. The null hypothesis of the test is H_o: $\frac{|\hat{x} - \hat{x}_i|_q}{\sigma_{q,i}} \sim N(0,1)$, and one can reject H_o in favour of the alternative hypnosis, and assume confirmation of a faulty observation(s) in mode *i*, if for any *k*:

$$\frac{|\hat{x} - \hat{x}_i|_k}{\sigma_{q,i}} \geq N_{\frac{\alpha 2}{2}}(0,1) \quad (13)$$

where $N_{\frac{\alpha 2}{2}}(0,1)$ is the test threshold computed as the inverse of the complement of the one-sided standard normal cumulative distribution function. Assuming the same total probability of false alarm ($\alpha 1$), and assuming that it is equally distributed for the Easting and Northing components; this gives $\alpha 2 = \frac{\alpha 1}{2 \times \text{number of fault modes}}$.

Typically, in RTK, code outliers are uncorrelated [25]; thus, if cycle slips are successfully detected and repaired the likelihood of a faulty measurement to mask another faulty measurement would be low. To confirm the exclusion of faulty measurements, we reapply the UMPI test and next a confirmation test is performed using the *w* test employing he normalised residuals, where for observation *j* we have [26]:

$$w_j = \frac{\hat{V}_j}{\sigma_{\hat{V}_j}} \quad (14)$$

$\sigma_{\hat{V}_j}$ is the standard deviation of $\hat{V}_j$ computed from the covariance matrix $Q_{\hat{V}}$. Assuming that the fault-free observations are Gaussian with zero-mean; the normalised residuals would consequently follow a standard normal distribution. Therefore, we confirm the exclusion of faulty observation *j* in mode *i* when:

$$|w_j| \geq N_{\frac{\alpha 3}{2}}(0,1) \qquad |w_j| \geq |w_l| \qquad \text{for } l\text{= 1 to } m \quad (15)$$

where $N_{\frac{\alpha 3}{2}}(0,1)$ is the inverse of the complement of standard normal distribution for $\frac{\alpha 3}{2}$. $\alpha 3$ is computed from the total significance level (α), which is assumed equally distributed among the observations; hence, $\alpha 3 = \alpha$/number of observations. α is computed using Baarda's B method [26], which assumes same probability for a type II error (failure to reject a false null hypothesis) in both the detection and identification tests.

The fault detection and exclusion (FDE) process described above is applied for the RTK mode. The measurements passing FDE next proceed to computation of the *PL*s. For detection of errors in the vehicle speed determined when using Doppler observations, the test using speed dilution of precession (SDOP) presented in [27] can be performed. For the case of positioning by using MEMS IMU heading + odometer speed that was presented earlier, there are no degrees of freedom. Accordingly, the FDE approach would not be possible and hence, the PL should be monitored. They should not exceed the alert limit. Computations of these PLs is subsequently discussed in the next section.

3.2. Computation of the protection level

For a moving vehicle one may consider its position along its direction of motion, and present this position in a vehicle-track specific reference frame. This 3D frame can be expressed by the along-track and cross-track horizontal position components and the vertical position [28, 29]. The position vector and its covariance matrix in the along-tack, cross-track and Up (AT-CT-U) frame, define as $v_{At-CT-U}$ and $Q_{At-CT-U}$ respectively, are computed from the position vector

and covariance matrix in the (E, N and U) frame (v_{E-N-U} and Q_{E-N-U}) by means of a clockwise rotation matrix R_θ, defined by the azimuthal direction of motion of the vehicle (θ, angle measured clockwise from North), where:

$$v_{At-CT-U} = R_\theta \, v_{E-N-U}$$
$$Q_{At-CT-U} = R_\theta^T \, Q_{E-N-U} \, R_\theta$$
$$\text{with} \quad R_\theta = \begin{bmatrix} \sin\theta & \cos\theta & 0 \\ \cos\theta & -\sin\theta & 0 \\ 0 & 0 & 1 \end{bmatrix} \tag{16}$$

The positioning errors, estimated as the difference between the true position and the estimated position, are typically unknown since the former is usually unspecified. Thus, the error should be bounded by the *PL*. We are generally not interested in the vertical component of the position in ITS applications; therefore, we restrict our focus only to the Horizontal *PLs*. for the AT-CT-U frame, the along-track *PL* (denoted as PL_{AT}) and cross-track *PL* (PL_{CT}) are considered. In practice, the PL_{AT} is of interest in applications such as forward-collision warning, which is a major collision risk, whereas PL_{CT} is of interest in carriage way departure alert and for lane identification of the vehicle, which is a key information parameter in ITS.

For the *AT* and *CT* positioning errors (denoted as dx_{AT} and dx_{CT}), respectively, the protection levels (PL_{AT} and PL_{CT}) should ensure that $P(|dx_{AT}| \geq PL_{AT}) \leq P(I)_{AT}$ and $P(|dx_{CT}| \geq PL_{CT}) \leq P(I)_{CT}$, where $P(I)_{AT}$ and $P(I)_{CT}$ are the the maximum allowable probability of risk (integrity risk) for AT and CT position components, which are set based on the application considered. In this contribution, we assume the same *PI* for AT and CT, such that $P(I)_{AT} = P(I)_{CT} = \frac{1}{2} P(I)_H$ where $P(I)_H$ is the horizontal integrity risk.

$P(I)_H$ is defined in terms of the conditioned probabilities and the probability of miss-detection as discussed in [14]. In RTK, ambiguity fixing has to be taken into consideration. Two events can take place, correct fixing (*CF*) and incorrect fixing (*IF*), with their probabilities expressed as P_{CF} and P_{IF}. The events are mutually exclusive and exhausting such that P_{IF} = 1 - P_{CF} [12]. Consequently, we consider integrity risk of combined probability of three cases. The first case accounts for miss-detection at an event where the ambiguities are correctly fixed and no errors are detected but the overall position error is larger than the *PL* resulting in flagging system integrity. The second case accounts for miss-detection when the carrier-phase ambiguities are wrongly resolved and the position error is larger than the *PL* when all satellites are used, and similarly for the third case but with removing satellite observation(s) in fault mode *i*. In our system, the above probabilities are evaluated using the method described in [11]. For the other two positioning systems, i.e. when using Doppler measurements and when using IMU-odometer measurements, we assume the same $P(I)_H$ to ensure the consistency of the system performance.

The *PL*s are modelled on the basis of the multi-hypothesis solution-separation method [8]. In RTK, with $df > 0$, a position error bound is computed for each possible fault mode (i) that might be miss-detected. This is performed by computing a position solution unaffected by the fault, by excluding the suspected observations and computing an error bound around this solution; and accounting for the difference between the position solution from all observations and the fault tolerant position [7, 14]. The PL_{AT} and PL_{CT} for fault mode *i* can be expressed as:

$$PL_{AT,i} = K_{fa,i} \; \sigma_{\delta AT,i} + K_{md,i} \; \sigma_{AT,i} + \sqrt{(\sin\theta \, a_1^T \, S_i \times \, b_o)^2 + \; (\cos\theta \, a_2^T \, S_i \times \, b_o)^2}$$
$$PL_{CT,i} = K_{fa,i} \; \sigma_{\delta CT,i} + K_{md,i} \; \sigma_{CT,i} + \sqrt{(\cos\theta \, a_1^T \, S_i \times \, b_o)^2 + \; (\sin\theta \, a_2^T \, S_i \times \, b_o)^2} \tag{17}$$

where σ_{AT} and σ_{CT} are the standard deviations for the AT and CT position components computed from $Q_{At-CT-U}$. $\sigma_{\delta AT,i}$ and $\sigma_{\delta CT,i}$ are estimated from σ_{dE_i}, σ_{dN_i} given in (10) of the sub-covariance matrix of (*E* and *N*) calculated from $(S - S_i)$ and using the covariance propagation law as shown in (16). b_o is a nominal GNSS observation bias, which is different for code and phase observations, and between systems (GPS, BeiDou, etc.). The biases can be attributed to antenna phase centre offset at the reference station, residual relative orbital and atmospheric errors, and hardware biases [30]. The absolute value of the bias is added to bound the worst case scenario and to ensure that the continuity requirement is met [16]. The case of a fault-free full set of observations is also considered by setting the fault mode *i* to zero. The final protection levels PL_{AT} and PL_{CT} are considered as the max$\{PL_{AT,i}\}$ and max$\{PL_{CT,i}\}$ respectively.

In this paper, integrity monitoring for RTK is computed using an epoch-by-epoch least-squares method after validation of the ambiguities. Accordingly, no dynamic model was used. Hence, the possibility of experiencing ramping errors due to the dynamic model errors from previous epochs affecting the current epoch were not taken into consideration. The use of Kalman filtering that takes this effect into consideration will be addressed in a future study.

The $K_{fa,i}$ and $K_{md,i}$ are scaling coefficients. Assuming that GNSS measurement noise is Gaussian with zero mean, the 2D position error after resolving the integer carrier-phase ambiguities can be considered as a random variable with a zero-mean Gaussian distribution. Hence, $K_{md,i}$ is the inverse of the complement of the one-sided standard normal cumulative distribution function (i.e. $K_{md,i} = -\mathrm{Q}^{-1}(\beta)$) to satisfy the miss-detection probability β, which can either be pre-set as explained in [14], and $K_{fa,i} = -\mathrm{Q}^{-1}\left(\frac{\alpha}{2m}\right)$ where we assume α=1% in this research.

When positioning using GNSS Doppler-measurements, where $df = 0$, the *PLs* are expressed as:

$$PL_{AT,i} = K_{md,i}\ \sigma_{AT,i} + \sqrt{(\sin\theta\ a_1^T\ S \begin{bmatrix} b_{v_E} \\ b_{v_N} \end{bmatrix})^2 + (\cos\theta\ a_2^T\ S \begin{bmatrix} b_{v_E} \\ b_{v_N} \end{bmatrix})^2}$$

$$PL_{CT,i} = K_{md,i}\ \sigma_{CT,i} + \sqrt{(\cos\theta\ a_1^T\ S \begin{bmatrix} b_{v_E} \\ b_{v_N} \end{bmatrix})^2 + (\sin\theta\ a_2^T\ S \begin{bmatrix} b_{v_E} \\ b_{v_N} \end{bmatrix})^2} \quad (18)$$

where b_{v_E} and b_{v_N} are assumed values for the nominal velocity biases in the Easting and Northing directions determined from Doppler measurements.

For the case of integrating the heading from MEMS IMU and speed of the odometer, where *df* = 0, the IMU heading bias should be frequently adjusted by other methods, such as GNSS-Doppler-based heading and ZUPT. The *PLs* are expressed as:

$$PL_{AT,i} = K_{md,i}\ \sigma_{AT,i} + \sqrt{(\sin\theta\ a_1^T\ S \begin{bmatrix} b_{\theta_{IMU}} \\ b_v \end{bmatrix})^2 + (\cos\theta\ a_2^T\ S \begin{bmatrix} b_{\theta_{IMU}} \\ b_v \end{bmatrix})^2}$$

$$PL_{CT,i} = K_{md,i}\ \sigma_{CT,i} + \sqrt{(\cos\theta\ a_1^T\ S \begin{bmatrix} b_{\theta_{IMU}} \\ b_v \end{bmatrix})^2 + (\sin\theta\ a_2^T\ S \begin{bmatrix} b_{\theta_{IMU}} \\ b_v \end{bmatrix})^2} \quad (19)$$

$b_{\theta_{IMU}}$ is a scalar representing possible unaccounted for IMU heading bias, whereby, the impact of this bias on positioning before IMU calibration, and its growth with time has to be considered. It is assumed here that this bias increases linearly with time, and hence, $b_{\theta_{IMU}} = b_{\theta_o} + \Delta b \times \Delta t$, where b_{θ_o} is the initial bias, Δb is the bias time-derivative, and Δt is the time difference between current epoch and the epoch at which the IMU was last calibrate. b_v is the bias attributed to velocity measured by the odometer.

As mentioned earlier, when positioning using Doppler measurements or when using IMU+odometer measurements, only time-changes of positions are measured. Consequently, the integrity risk has to take into account the accumulation of errors with time in addition to the possibility of experiencing instantaneous faults. The parametric equation for these cases can be presented as:

$$\begin{bmatrix} E_t \\ N_t \end{bmatrix} = \frac{\Delta t}{2} \begin{bmatrix} 1 & 0 & 1 & 0 \\ 0 & 1 & 0 & 1 \end{bmatrix} \begin{bmatrix} v_{E_{t-1}} \\ v_{N_{t-1}} \\ v_{E_t} \\ v_{N_t} \end{bmatrix} + \begin{bmatrix} E_{t-1} \\ N_{t-1} \end{bmatrix} \quad (20)$$

where Δt is the time difference between t and t-1. The covariance matrix of the unknown coordinates (Q_{EN_t}) is then given as:

$$Q_{EN_t} = A\ Q_{obs}\ A^T + Q_{EN_{t-1}} \quad (21)$$

where $A = \frac{\Delta t}{2} \begin{bmatrix} 1 & 0 & 1 & 0 \\ 0 & 1 & 0 & 1 \end{bmatrix}$ and the initial covariance matrix is taken from the covariance matrix of the initial position, determined from RTK. To limit the development of the accumulated error, this positioning approach needs to be reinitialized at short time intervals, for instance using RTK. The Q_{EN_k} is re-set with this re-initialization. Such approach will result in a sawtooth-like pattern for the *PL* to adapt to the growth-reset error behaviour, as will be shown in the next sections. The $Q_{(At-CT)_t}$ is computed from Q_{EN_t} by applying the covariance propagation law using the 2D rotation matrix $R_\theta = \begin{bmatrix} \sin\theta & \cos\theta \\ \cos\theta & -\sin\theta \end{bmatrix}$.

For the three positioning methods discussed so far, the accuracy requirement is selected at 95% confidence level and is evaluated by:

$$\text{Accuracy}_{AT}(95\%) = K_{acc}\ \sigma_{AT} < T_{acc\text{-}AT}$$
$$\text{Accuracy}_{CT}(95\%) = K_{acc}\ \sigma_{CT} < T_{acc\text{-}CT},$$
taking K_{acc} = 1.96. (22)

where $T_{acc\text{-}AT}$ and $T_{acc\text{-}CT}$ are the accuracy threshold for the AT and CT position components, to be set according to the application considered. RTK typically provides accuracy < 5 cm, whereas the Doppler-based and IMU+odometer positioning can only provide sub-m accuracy for short periods of operation, which may grow to several metres for longer operational periods when left without calibration.

4. Testing

A kinematic test was conducted to evaluate the proposed method where a small vehicle was used fitted with RTK system, and a Bosch-consumer grade MEMS IMU. The test is performed in a dense urban environment in Tokyo, Japan that includes several multi-story buildings. The test trajectory is shown in Figure 2. The RTK system used GPS, GLONASS and BeiDou dual-frequency observations of 10 Hz sampling interval. The heading error of the used MEMS IMU ranged from -2º to 5º, which can accumulate to 10º after 30 min without calibration [14]. Our previous examination of this IMU system has shown that it has a zero bias in the static mode, but in the kinematic mode, the bias can reach approximately 0.004º/s. For the odometer, the standard deviation of the computed speed is estimated as 5 cm/s, and for the speed determined from GNSS-Doppler measurements it is 10 cm/s.

The positioning error (*PE*) in the RTK mode was estimated as the difference between RTK positions with those determined from post-mission kinematic processing (PPK) of the same data using independent software (Trimble Business Centre). A comparison between the two approaches in a pre-rest static mode showed that no software-bias was present. The positioning errors for the two other cases, firstly when using

Doppler measurements and secondly when using IMU+odometer were computed by differencing their positions with the output from a POS/LV system (developed by Applanix Inc.), which was mounted on the vehicle and has a nominal positioning accuracy equals 20 cm.

Possible values for horizontal alert limit (*HAL*) and integrity risk (β) for ITS, which are expected to be application dependent, are currently under investigation by various research groups and transport authorities. Since no standards are available yet, the *PL*s in our tests were computed using a range of values of β ranging between 1×10^{-3} and 1×10^{-6} in order to experimentally show the effect of setting a certain value of β on integrity monitoring results. An 99% integrity availability is aimed for RTK using (α) of 0.01.

Fig. 2. Test trajectory in Tokyo

5. Results

Positioning using a system of combined RTK, Doppler and IMU+odometer is carried out following the work-order described in Figure 1, and provided that the set conditions specified in Table 1 are satisfied. Results show that positioning was available during the entire test period. RTK was available for 72.2% of the test trajectory with outages ranging from 1s to 49.2s, where positioning is bridged by Doppler-based positioning for 25.8% of the test period. The IMU+odometer method was required for for short periods ranging between 0.5s and 4s, totalling 2% of the full period.

Figures 3 and 4 show the time series of *PL* during the whole test period for the along-track and cross-track directions (shown as *PL_AT* and *PL_CT*) and the absolute values of the positioning errors along these directions, denoted as *err_AT* and *err_CT*, and using an integrity risk of 1×10^{-4} and 1×10^{-6} as examples. The *PE* and *PL* for different systems are shown, such that the results of the combined systems are given first in the top panel of the figures, next RTK results are illustrated in the 2nd panel. In the 3rd panel, Doppler results are depicted, and lastly the IMU+odometer positioning results are shown at the bottom panel of the figures. For a better demonstration of the RTK results, the error scale is set smaller (0.5m) in the relevant figures than the rest of the sub-figures.

The obtained positioning accuracy using different methods is expressed in terms of the position errors computed by referencing each of them to a more precise method as explained above. Table 2 shows the median of the absolute positioning errors and the RMSE for each mode. The table and the Figures 3 and 4 show that the RTK with correct ambiguity resolution provided positioning errors of a few cm. Positioning using Doppler measurements and IMU+odometer provided sub-m level accuracy when they were employed for short periods, which was less than 50s for Doppler and less than 5s for IMU+odometer. For longer periods the error may reach several meters. Consequently, positioning using Doppler measurements was reinitialized every one minute. For the corresponding *PLs*, the sawtooth pattern, discussed earlier, resulting from the accumulation of errors until the system is reinitialized is shown in the figures. Similarly, the ramping accumulated heading biases between IMU calibrations dominated the behaviour of this positioning mode as depicted in the Figures 3 and 4. In general, positioning by a low-cost MEMS IMU gave the worst accuracy compared to the two other positioning approaches, where the error reached 0.53m after 4s, which can grow to more than 2 m in less than 20s if left without calibration. Hence, this method should be restricted to bridging positioning by RTK only for very short periods. The other option is to use an IMU of a better grade. Note here that the results of Table 2 refer to the use of Doppler measurements for up to 49 sec, whereas the results of IMU+odometer were limited to its use for up to 4 sec, which explains why results from the former appear to be worse than the latter. For a similar period of operation, the MEMS IMU will accumulate more errors.

Fifteen faulty code measurements have been detected and isolated, which may be caused by high multipath in this high-density urban environment. In addition, the figures show that there were a few cases where the ambiguity resolution appears to be incorrectly fixed by a few cycles. However, the computed *PLs* sensed this behaviour through the escalation in standard deviations and consequently were increased to bound this error. In general, RTK with correct ambiguity resolution generally yield positioning of a few cm errors. Such errors will be bounded by tight protection levels and inspection of the Figures shows that an Alert Limit (*AL*) can be safely chosen as 1m.

Recall that in integrity monitoring we check that the position error (*PE*) is bounded by *PL* and *PL* should be lower than *AL*. Analysis of the results demonstrated that the positioning errors were always bounded by the protection levels during the test period (i.e. *PE*<*PL*<*AL*) for the full period of RTK positioning and when positioning using Doppler measurements, as well as during the majority of IMU+odometer positioning, which gave a total availability of integrity monitoring > 99%. These results verify the initial validation of the proposed method.

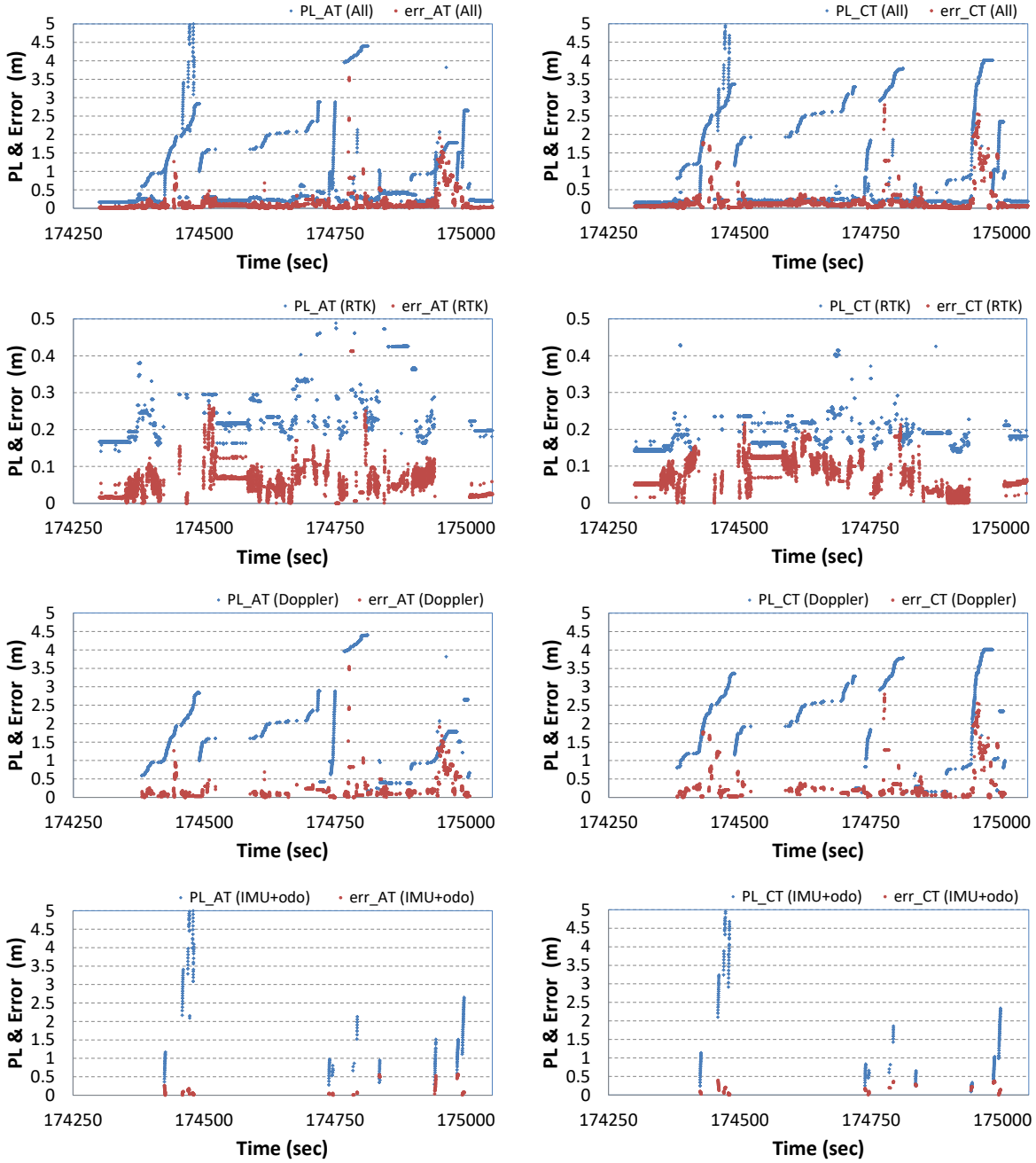

Fig. 3. *PL_AT*, *PL_CT* and *positioning errors for the AT (left) and CT (right)* for the combined systems (top panel), RTK (2nd panel), Doppler Positioning (3rd panel), and IMU+odometer positioning (bottom panel), *integrity risk*= 1×10^{-4}.

Table 2. Median positioning error and RMSE for *AT* and CT directions (m)

Positioning mode	Median Error		RMSE	
	(AT)	(CT)	(AT)	(CT)
RTK	0.058	0.054	0.077	0.105
Doppler	0.163	0.172	0.332	0.442
IMU+odometer	0.150	0.321	0.249	0.206

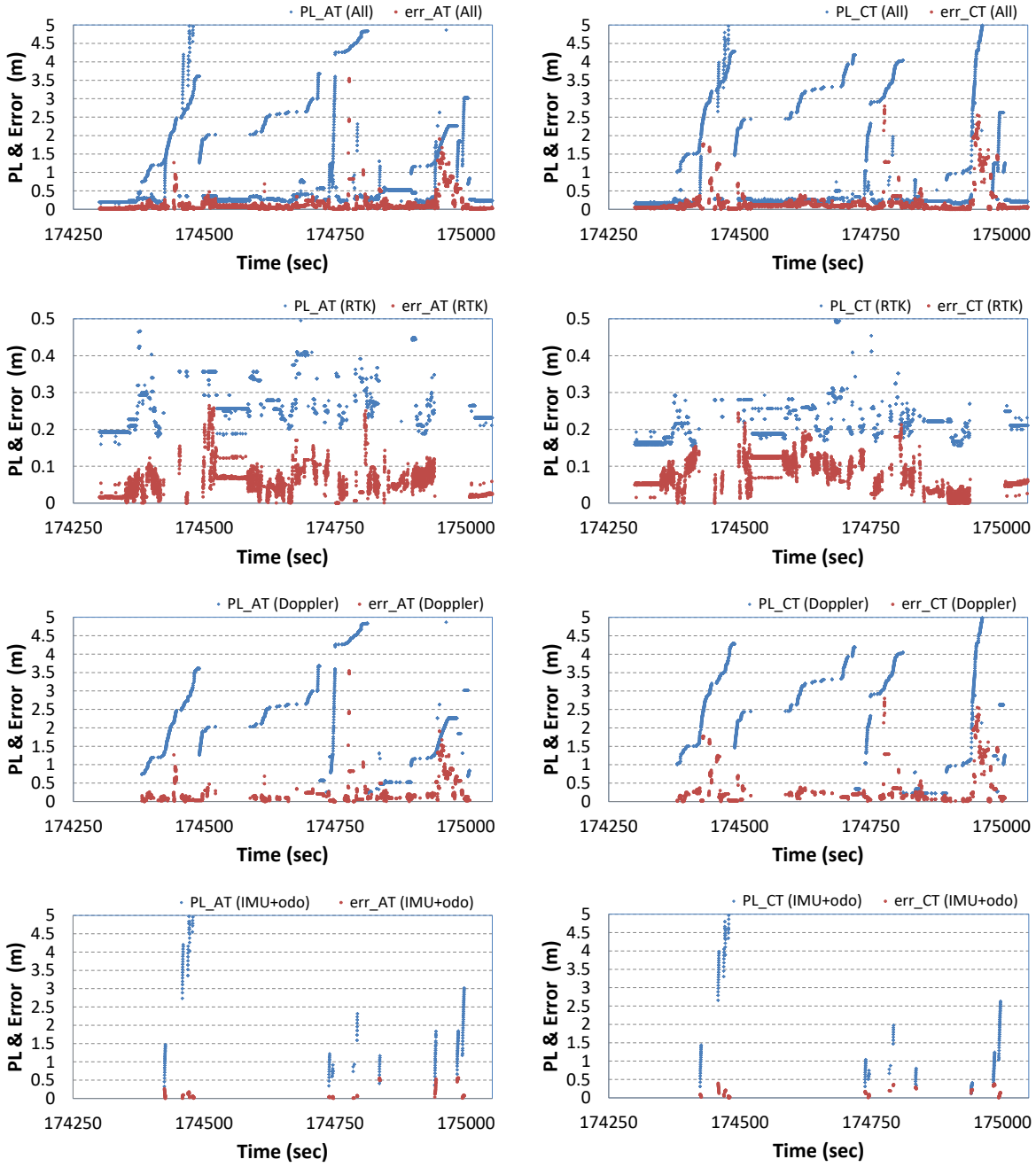

Fig. 4. *PL_AT*, *PL_CT* and *positioning errors for the AT (left) and CT (right)* for the combined systems (top panel), RTK (2nd panel), Doppler Positioning (3rd panel), and IMU+odometer positioning (bottom panel), *integrity risk*= 1×10^{-6}.

The median of the *PL* for the AT and CT directions using different approaches are given in the Tables 4 and 5. The median is used in place of the mean value as the former is less affected by outliers and skewed values of *PLs* as discussed in [14]. The Tables show that *PLs* increase with the reduction of the allowed integrity risk. This can also be seen by comparing the Figures 3 and 4. This increase in *PLs* is attributed to the fact that the decrease of the integrity risks (probability) amplifies the scaling factor used in the *PL* models. When the *PL* exceeds the *AL* (which should be selected according to the application at hand) integrity monitoring is affirmed as unavailable. Thereby, the increase of the integrity risks can lead to significant unavailability of IM, and hence, this value should be carefully selected.

Table 4. Median *PL_AT* using different positioning modes and different values of integrity risk (m)

Integrity risk	1×10^{-3}	1×10^{-4}	1×10^{-5}	1×10^{-6}
RTK	0.176	0.197	0.215	0.232
Doppler	1.355	1.621	1.851	2.057
IMU+odometer	1.208	1.368	1.506	1.601

Table 5. Median *PL_CT* using different positioning modes and different values of integrity risk (m)

Integrity risk	1×10^{-3}	1×10^{-4}	1×10^{-5}	1×10^{-6}
RTK	0.148	0.164	0.177	0.188
Doppler	1.802	2.159	2.468	2.623
IMU+odometer	0.884	1.101	1.150	1.191

6. Conclusion

A new integrity monitoring (IM) methodology is presented for a proposed system that can be used for intelligent transportation systems (ITS). The system includes GNSS RTK integrated with low-cost MEMS IMU and automotive odometer. A new approach for computation of the protection levels is discussed for each of the three positioning modes. These protection levels bound the positioning errors for the direction of movement of the vehicle (along-track), which is of interest for collision avoidance, and for the cross-track direction, needed for lane identification.

Pilot testing of the proposed system was carried out in a dense urban area, which is a challenging environment for ITS applications. Results proved initial validity of the proposed integrity monitoring method. For RTK with correct ambiguity resolution, tight *PLs* were created and an alert limit of 1 m can be safely used with IM availability larger than 99%. This can support several ITS applications. Positioning using Doppler measurements or using IMU+vehicle odomter can bridge short breaks of RTK. However, as these methods compute the time-change in positioning and their errors and biases accumulate with time, they need frequent calibration. Their bridging of positioning is thus recommended only for a few seconds, where sub-meter accuracy can be obtained. Since standards for selection of integrity risk in ITS are not yet defined, which could be application dependent, testing of the proposed system and IM methodology was performed using several values, ranging from 1×10^{-3} to 1×10^{-6}. This is to experimentally show the effect of selecting the integrity risk on the outcomes. Results showed that the protection levels increased with the decrease of the allowable integrity risk, which can lead to significant unavailability of IM. Thus, careful selection of this value is needed while satisfying the application positioning continuity requirements. Our future work includes investigating the use of a higher-grade IMU that can be afforded by the automotive industry and implementation of the algorithms in a Kalman filtering data processing scheme.

Acknowledgment

This study is partially supported by the Australian Research Council grant number DP170103341 to the first author.

References

[1] Imparato, D., El-Mowafy, A., Rizos, C. and Wang, J.: A review of SBAS and RTK vulnerabilities in Intelligent Transport Systems applications, *Proceedings IGNSS Symposium 2018*, Sydney, 7–9 Feb 2018, 1-18.

[2] Yang Y, Mao X, Tain W.: A Novel Method for Low-Cost MIMU aiding GNSS Attitude Determination *Measurement Science and Technology*, 2016, 27(7), 075003.

[3] Yand L, Wu Y, Li Y, Rizos C.: An enhanced MEMS-INS/GNSS integrated system with fault detection and exclusion capability for land vehicle navigation in urban areas *GPS Solutions*, 2014, 18(4) 593-603.

[4] Misra P, Enge P.: *Global Position System: Signals, Measurements, and Performance*. Ganga-Jamuna Press. 2006.

[5] Zumberge, J. F., Heflin M. B., Jefferson D.C., Watkins M. M. Webb F. H.: Precise Point Positioning for The Efficient and Robust Analysis of GPS Data from Large Networks, Journal of Geophysical Research, 1997, 102, B3, 5005-17.

[6] Kouba, J.: A Guide to using International GNSS Service (IGS) Products, https://kb.igs.org/hc/en-us/articles/201271873-A-Guide-to-Using-the-IGS-Products, 2015, Accessed Dec 2017.

[7] El-Mowafy A.: Pilot Evaluation of Integrating GLONASS, Galileo and BeiDou with GPS in ARAIM *Artificial Satellites*, 2016, 51(1) 31-44.

[8] Blanch, J, Walter T, Enge P.: Optimal Positioning for Advanced RAIM *Navigation*, 2014, 60(4) 279-289.

[9] Rippl M, Martini I, Belabbas B, Michael M 2014 ARAIM Operational Performance Tested in Flight *Proc. of ION ITM 2014* San Diego CA 27-29 Jan 2014, 601-615.

[10] El-Mowafy A, Yang C.: Limited Sensitivity Analysis of ARAIM Availability for LPV-200 over Australia using real data *Advances in Space Research*, 2016, 57(2) 659–670.

[11] Khanafesh S, Pervan P.: New Approach for Calculating Position Domain Integrity Risk for Cycle Resolution in Carrier Phase Navigation Systems, *IEEE Trans. on Aerospace and Electronic systems*, 2010, 46(1) 296-306.

[12] Khanafesh S, Langel S.: Implementation and Experimental Validation of Cycle Ambiguity Resolution with Position Domain Integrity Risk Constraints *Navigation,* 2011, 58(1) 45-58.

[13] Cezón A, Cueto M, Fernández I.: Analysis of Multi-GNSS Service Performance Assessment: ARAIM vs. IBPL Performances *Proc. ION GNSS 2013 Nashville* 16-20 September 2013, 2654 – 2663.

[14] El-Mowafy, A., Kubo N.: Integrity Monitoring of Vehicle Positioning in Urban Environment Using RTK-GNSS, IMU and Speedometer. *Measurement, Science and Technology,* 2017, 28(5), 055102, 1-12.

[15] Imparato, D., El-Mowafy, A., Rizos, C. and Wang, J.: A review of SBAS and RTK vulnerabilities in Intelligent Transport Systems applications, Proc. IGNSS Symposium 2018, Sydney, 7 – 9 February 2018, 1-18.

[16] El-Mowafy A.: Performance Analysis of the RTK Technique in an Urban Environment *the Australian Surveyor (currently J. of Spatial Sciences),* 2000, 45(1) 47-54.

[17] El-Mowafy A.: Precise Real-Time Positioning Using Network RTK, Book: *Global Navigation Satellite Systems: Signal, Theory and Applications*. 2012, Chapter 7, pp.161-188, *InTech*. ISBN: 978-953-307-674-4.

[18] Godha S, Canon ME.: GPS/MEMS INS integrated system for navigation in urban areas, *GPS Solutions,* 2007, 11(3) 193-203.

[19] El-Sheimy N, Hou H, Niu X.: Analysis and Modeling of Inertial Sensors Using AV, *IEEE Transaction on instrumentation and measurement,* 2008, 57(1) 140-149.

[20] Zhao Y.: *GPS/IMU Integrated System for Land Vehicle Navigation based on MEMS*. Thesis, Royal Institute of Technology, Stockholm, Sweden, 2011.

[21] Estey L, Meertens C.: TEQC: The Multi-purpose Toolkit for GPS/GLONASS Data, *GPS Solutions,* 1999, 3(1) 42-49.

[22] Vaclavovic P, Dousa J.: G-nut's Anubis – open-source tool for multi-GNSS data checking and editing, *Proc. of IAG Scientific Assembly,* Potsdam September 1–6 2013, 1-7.

[23] El-Mowafy A.: GNSS Multi-frequency Receiver Single-Satellite Measurement Validation Method *GPS Solutions,* 2014, 18 553-561.

[24] Teunissen PJG.: *T esting theory: an introduction*. 2nd ed., Delft VSSD The Netherlands. 2006.

[25] El-Mowafy A.: Diagnostic Tools Using a Multi-Constellation Single-Receiver Single-Satellite Data Validation Method *J. of Navigation,* 2015, 68(1) 196-214.

[26] Baarda WA.: *Testing Procedure for Use in Geodetic Networks* Netherlands Geodetic Commission, Publications on Geodesy, New Series 1968, 2(5).

[27] Chalko, TJ.: Estimating Accuracy of GPS Doppler Speed Measurement Using Speed Dilution of Precision Parameter, *NU Journal of Discovery,* 2009, 6 4-9.

[28] Imparato, D., El-Mowafy, A., Kubo, N.: Integrity Assessment of Vehicle Positioning for Journey Planning in Urban Environment using RTK and 3D City Models. *J. of Intelligent Transport Systems: Technology, Planning, and Operations*. 2018b

[29] Margaria, D. and Falletti, E.: A novel local integrity concept for GNSS receivers in urban vehicular contexts. *In Proceedings of the IEEE/ION PLANS 2014*, Monterey, CA, USA, 5-8 May, 2014, 413-425.

[30] El-Mowafy A, Deo M, Rizos C.: On Biases in Precise Point Positioning with Multi-Constellation and Multi-Frequency GNSS Data. *Measurement Science and Technology,* 2016, 27(3), 035102.